



Deposited via The University of York.

White Rose Research Online URL for this paper:

<https://eprints.whiterose.ac.uk/id/eprint/106697/>

Version: Accepted Version

Article:

Cavada, Nathalie, Ciolli, Marco, Barelli, Claudia et al. (2017) Integrating field and satellite data for spatially explicit inference on the density of threatened arboreal primates.

ECOLOGICAL APPLICATIONS. pp. 235-243. ISSN: 1051-0761

<https://doi.org/10.1002/eap.1438>

Reuse

Items deposited in White Rose Research Online are protected by copyright, with all rights reserved unless indicated otherwise. They may be downloaded and/or printed for private study, or other acts as permitted by national copyright laws. The publisher or other rights holders may allow further reproduction and re-use of the full text version. This is indicated by the licence information on the White Rose Research Online record for the item.

Takedown

If you consider content in White Rose Research Online to be in breach of UK law, please notify us by emailing eprints@whiterose.ac.uk including the URL of the record and the reason for the withdrawal request.



Integrating field and satellite data for spatially-explicit inference on the density of threatened

arboreal primates



Journal:	<i>Ecological Applications</i>
Manuscript ID	EAP16-0224.R1
Wiley - Manuscript type:	Articles
Date Submitted by the Author:	n/a
Complete List of Authors:	Cavada, Nathalie; Universita degli Studi di Trento, DICAM; MUSE - Museo delle scienze, Tropical biodiversity section Ciolli, Marco; Universita degli Studi di Trento, DICAM Rocchini, Duccio; Fondazione Edmund Mach, Research and innovation centre, Biodiversity and Molecular Ecology Department Barelli, Claudia; MUSE - Museo delle scienze, Tropical biodiversity section Marshall, Andrew; University of York, CIRCLE, Environment Department; Flamingo Land Ltd. Rovero, Francesco; MUSE - Museo delle Scienze, Tropical biodiversity section
Substantive Area:	Statistics and Modeling < Theory < Substantive Area, Spatial Statistics and Spatial Modeling < Statistics and Modeling < Theory < Substantive Area, Endangered Species < Management < Substantive Area, Reserves/Protected Areas < Management < Substantive Area, Remote Sensing < Methodology < Substantive Area, Conservation < Landscape < Substantive Area
Organism:	Mammals < Vertebrates < Animals, Primates < Mammals < Vertebrates < Animals, Plants
Habitat:	Tropical Zone < Terrestrial < Habitat, Rain Forest < Tropical Zone < Terrestrial < Habitat
Geographic Area:	Africa < Geographic Area, East Africa < Africa < Geographic Area
Additional Keywords:	abundance, basal area, GIS, Landsat, primates, remote sensing, spatially explicit models, tropical forest, Udzungwa
Abstract:	Spatially explicit models of animal abundance are a critical tool to inform conservation planning and management. However, they require the availability of spatially diffuse environmental predictors of abundance, which may be challenging especially in complex and heterogeneous habitats. This is particularly the case for tropical mammals, such as non-human primates, that depend on multi-layered and species-rich tree canopy coverage, which is usually measured through a limited sample of

ground plots. We developed an approach that calibrates remote-sensing imagery to ground measurements of tree density to derive basal area, in turn used as a predictor of primate density based on published models. We applied generalized linear models (GLM) to relate 9.8 ha ground samples of tree basal area to various metrics extracted from Landsat 8 imagery. We tested the potential of this approach for spatial inference of animal density by comparing the density predictions for an endangered colobus monkey, to previous estimates from field transect counts, measured basal area, and other predictors of abundance. The best GLM had high accuracy and showed no significant difference between predicted and observed values of basal area. Our species distribution model yielded predicted primate densities that matched those based on field measurements. Results show the potential of using open-access and global remote sensing data to derive an important predictor of animal abundance in tropical forests and in turn to make spatially explicit inference on animal density. This approach has important, inherent applications as it greatly magnifies the relevance of abundance modeling for informing conservation. This is especially true for threatened species living in heterogeneous habitats where spatial patterns of abundance, in relation to habitat and/or human disturbance factors, are often complex and, management decisions - such as improving forest protection - may need to be focused on priority areas.

Note: The following files were submitted by the author for peer review, but cannot be converted to PDF. You must view these files (e.g. movies) online.

DataS1.csv

SCHOLARONE™
Manuscripts

View Only

1 **Integrating field and satellite data for spatially-explicit inference on the density of threatened**
2 **arboreal primates**

3

4 Nathalie Cavada^{1,2}, Marco Ciolli¹, Duccio Rocchini³, Claudia Barelli², Andrew R. Marshall^{4,5},

5 Francesco Rovero^{2,6}

6

7 ¹DICAM Department of Civil, Environmental and Mechanical Engineering, University of Trento,

8 Trento, Italy.

9 ²Tropical Biodiversity Section, MUSE - Museo delle Scienze, Trento, Italy.

10 ³Biodiversity and Molecular Ecology Department, Research and Innovation Centre – Fondazione

11 Edmund Mach, San Michele all'Adige, Italy.

12 ⁴CIRCLE, Environment Department, University of York, York, United Kingdom.

13 ⁵Flamingo Land Ltd., Kirby Misperton, North Yorkshire, York, United Kingdom.

14 ⁶Udzungwa Ecological Monitoring Centre, Udzungwa Mountains National Park, Mang'ula,

15 Tanzania.

16

17 Correspondence: Nathalie Cavada, DICAM Department of Civil, Environmental and Mechanical

18 Engineering, University of Trento, Via Mesiano 77, 38123 Trento, Italy.

19 Phone: +393404122810; E-mail: nathalie.cavada@unitn.it

20

21 Keywords: abundance; basal area; GIS; Landsat; primates; remote sensing; spatially explicit

22 models; tropical forest; Udzungwa.

23 Abstract

24 Spatially explicit models of animal abundance are a critical tool to inform conservation planning
25 and management. However, they require the availability of spatially diffuse environmental
26 predictors of abundance, which may be challenging especially in complex and heterogeneous
27 habitats. This is particularly the case for tropical mammals, such as non-human primates, that
28 depend on multi-layered and species-rich tree canopy coverage, which is usually measured through
29 a limited sample of ground plots. We developed an approach that calibrates remote-sensing imagery
30 to ground measurements of tree density to derive basal area, in turn used as a predictor of primate
31 density based on published models. We applied generalized linear models (GLM) to relate 9.8 ha
32 ground samples of tree basal area to various metrics extracted from Landsat 8 imagery. We tested
33 the potential of this approach for spatial inference of animal density by comparing the density
34 predictions for an endangered colobus monkey, to previous estimates from field transect counts,
35 measured basal area, and other predictors of abundance. The best GLM had high accuracy and
36 showed no significant difference between predicted and observed values of basal area. Our species
37 distribution model yielded predicted primate densities that matched those based on field
38 measurements. Results show the potential of using open-access and global remote sensing data to
39 derive an important predictor of animal abundance in tropical forests and in turn to make spatially
40 explicit inference on animal density. This approach has important, inherent applications as it greatly
41 magnifies the relevance of abundance modeling for informing conservation. This is especially true
42 for threatened species living in heterogeneous habitats where spatial patterns of abundance, in
43 relation to habitat and/or human disturbance factors, are often complex and, management decisions
44 - such as improving forest protection - may need to be focused on priority areas.

45

46 Introduction

47 Species abundance estimation and the identification of factors predicting its variation is a pervasive
48 goal in ecology and conservation biology and it is gaining increasing attention through the emergent
49 potential of spatially explicit modeling (Guisan and Zimmermann 2000, Guisan and Thuiller 2005,

50 Wulder and Franklin 2006, Anadón et al. 2010). This is particularly true for threatened species
51 living in heterogeneous landscapes, where habitat structure and human disturbance vary according
52 to complex spatial patterns. In these contexts, inference on abundance becomes truly informative
53 only when it accounts for such heterogeneity (Arroyo-Rodríguez and Fahrig 2014). Human-
54 modified landscapes are also expanding in tropical areas, where forest fragmentation, degradation
55 and defaunation strongly affect species viability (Balmford and Whitten 2003, Arroyo-Rodríguez
56 and Fahrig 2014). However, because of limited and substandard data, spatially explicit models are
57 less exploited in tropical areas compared to temperate ones (Cayuela et al. 2009). Thus, integrating
58 the use of field data with remote sensing data represents an advantageous approach to ensure data
59 quality for spatial modeling in these areas (Wilkie and Finn 1996, Proisy et al. 2007).

60

61 Remote sensing data (especially Landsat) have been used to investigate several ecological
62 questions, mainly related to land cover change, carbon storage and habitat mapping (Schroeder et
63 al. 2011, Legaard et al. 2015, Mayes et al. 2015, Twongyirwe et al. 2015). However, the resolution
64 and quality of Landsat data do not always adequately represent environmental components that are
65 most important for target species, such as vegetation structure, because optical satellite imagery is
66 not three-dimensional (Hall et al. 1995, Duncanson et al. 2010). Therefore, methods are needed to
67 characterize features of the forest structure that are relevant to target species, particularly for
68 inaccessible areas where Landsat images represent the only feasible option.

69

70 In this study, we aimed to derive arboreal primate density from remote sensing estimates of 'tree
71 stem basal area'. Basal area is typically related to canopy cover (Alexander 1971, Farr et al. 1989,
72 Smith et al. 1992), but the two measures are not directly interchangeable (Cade 1997). In particular,
73 mean basal area specifically measures the contribution of each tree to biomass and hence identifies
74 forest structure, succession stage and disturbance. Accordingly, it is a common measure of habitat
75 quality for predicting animal abundance (Braithwaite et al. 1989, Medley 1993, Umapathy and
76 Kumar 2000). This is especially true for non-human primates (Mbora and Meikle 2004, Cristóbal-

77 Azkarate et al. 2005, Anderson et al. 2007, Struhsaker and Rovero 2007) which are globally
78 threatened and in urgent need of conservation actions (Schipper et al. 2008, Schwitzer et al. 2015).
79 Our specific objectives were to: a) model measured basal area against a combination of different
80 metrics and indices derived from Landsat imagery; b) test the performance of the best-performing
81 model to predict values of basal area outside of the sampled areas; c) use the results to derive a
82 spatial map of population density of the endangered (IUCN 2015) Udzungwa red colobus monkey
83 (*Procolobus gordonorum*), based on previously published density-basal area model; d) compare the
84 modeled primate density to previous predictions from field measurements; e) further refine these
85 estimates using environmental and human predictors.

86

87 **Materials and Methods**

88 **Study area**

89 The Udzungwa Mountains are located in the south-central part of Tanzania and represent the largest
90 mountain bloc in the Eastern Arc Mountains, covering an area larger than 19,000 km² (Platts et al.
91 2011). Closed forest blocs, ranging in size from 12 to over 500 km² (Marshall et al. 2010), are
92 interspersed with drier habitats. We focused our study on the forest of Mwanihana, one of the largest
93 forest blocs (150.6 km²) and under the protection of the Udzungwa Mountain National Park
94 (UMNP) since 1992. Highly variable habitat types are distributed along the altitudinal gradient of
95 the forest ranging from 351 to 2,263 m a.s.l. Deciduous forest is found in the lowland, with semi-
96 deciduous and evergreen forests covering the sub-montane and montane areas, while *Hagenia* and
97 bamboo-dominated forest characterize the upper montane level (Lovett et al. 2006). Woody
98 vegetation density increases with elevation, with the largest trees found at mid elevation, probably a
99 result of human disturbance and tree respiration costs (Marshall et al. 2012).

100

101 **Vegetation data**

102 We derived field data for tree stems ≥ 10 cm DBH (Diameter at Breast Height; 1.3m) from three
103 sources (Fig. 1): (1) From the Tropical Ecology Assessment and Monitoring Network (TEAM)

104 (<http://www.teamnetwork.org/>, dataset ID 0327011905 4443), comprising six vegetation plots of
105 100 × 100m on a horizontal plane (i.e. adjusted for slope), following a standardized protocol
106 (TEAM Network 2011); (2) 153 vegetation plots of 25 × 25m, sampled along line transects
107 uniformly distributed in the forest (from Barelli et al. 2015); (3) 33 new randomly placed vegetation
108 plots of 25 × 25m, sampled in June-July 2015, stratified according to the predominant habitat
109 gradient from disturbed lowland deciduous to mature montane evergreen forest. All newly-sampled
110 plots were placed in the centre of Landsat pixels for concordance with our remote-sensing imagery.
111 A summary of the vegetation data sets is provided in Data S1.

112 We obtained a single, cloud free, L8 OLI/TIRS Landsat image (Landsat scene ID
113 LC81670652014299LGN00, courtesy of the U.S. Geological Survey), acquired October 26, 2014.
114

115 **Primate density data**

116 Density data on the Udzungwa red colobus from across the study area were obtained from an earlier
117 study (Cavada et al. 2016). This study used environmental covariates from the 153 plots established
118 by Barelli et al. (2015) and distance sampling along line transects, to estimate colobus density
119 across the study area. Transect data were modeled as a hierarchical coupled logistic regression,
120 assuming a Poisson distribution for the animal abundance at a transect level. The detection process
121 of the distance sampling was modeled according to a multinomial distribution, assuming a
122 monotonical decrease of the detection probability with the increasing distance of the animal groups
123 from the observer. The influence of a series of environmental and human disturbance covariates was
124 evaluated and incorporated on both the abundance and detection steps in the model. Final density
125 estimates at the plot level were derived from environmental correlates that included mean basal
126 area, elevation and distance from disturbance (i.e. forest edge), that were found to significantly
127 affect the abundance and detectability of the red colobus in the study area.

128

129 **Analysis**

130 **Landsat metrics and vegetation indices**

131 To model basal area we first derived various Landsat metrics (Table 1). This began with a Principal
132 Component Analysis (PCA) to extract uncorrelated information from the different spectral bands
133 provided by the Operational Land Imager (OLI) sensor of the Landsat 8 satellite. After applying
134 PCA we further compressed the spectral data applying the Tasseled Cap Transformation (TCT) to
135 represent forest structure (Cohen et al. 1995). We also used a GRASS module (Neteler et al. 2012),
136 modified to derive vegetation-related spectral indices, combining specific bands of the Landsat 8
137 satellite images (Data S2). Such indices enhance the signal related to vegetation, while minimizing
138 background edaphic, solar and atmospheric effects (Jackson and Huete 1991).

139

140 **Model building**

141 To relate field sampled values of basal area to the metrics calculated from the Landsat images, we
142 used all newly-sampled plots, plus a subsample of the TEAM and Barelli et al. (2015) plots. The
143 subsample plots were those showing at least 75% overlap with Landsat pixels (N=115). In each plot
144 we calculated the basal area (BA, m²) for each sampled tree (DBH ≥10cm) as $BA = \pi * (DBH/2)^2$. We
145 then derived the mean basal area (MBA) for each plot, for use as the response variable (following
146 Barelli et al. (2015) and Cavada et al. (2016)).

147

148 We used generalized linear modeling (GLM) to investigate the relationship between the MBA- field
149 sampled values and the Landsat metrics and indices. Prior to building the models we checked for
150 the presence of collinearity among predictor variables to remove those providing identical
151 information. We thus calculated Variance Inflation Factor (VIF), using a cut off value of 10
152 (Marquardt 1970, Hair et al. 2006, Kennedy 2008) and we retained the uncorrelated predictors P1,
153 P2, RGI, RR, SLAVI. From an Empirical Cumulative Distribution Function (ECDF) of the response
154 variable, we decided to use an inverse Gaussian error distribution for the GLM with an inverse
155 squared link function (Fig. 2).

156

157 We built models using all the possible combinations of the retained Landsat predictors and we used
158 the Akaike Information Criterion (AIC) to rank the candidate models. We considered those models
159 showing $\Delta AIC < 2$ as equivalent (Anderson and Burnham 2002) and defined an average model by
160 determining Akaike weights (w_i) for each of the best models, using the packages ‘AICcmodavg’
161 (Mazerolle 2015) and ‘MUMin’ (Barton 2014) in R version 3.2.1 (R Core Team 2015). For
162 validating the model we randomly split the MBA dataset into two subsets, one for model fitting
163 with 75% of the data (N=109) and one with the remaining 25% of the data (N=37). We then used
164 bootstrapping to verify the goodness of fit of the selected average model: we simulated 1,000
165 datasets from the subset derived for model fitting (i.e the one considering 75% of the data) and then
166 defined a function that returned the fit-statistic Pearson χ^2 . We validated the model by checking the
167 distribution of the residuals for the validation subset. We evaluated model bias by comparing both
168 observed and predicted values, to a null model of mean residual prediction equal to zero, using
169 Wilcoxon's signed rank test (for $\alpha=0.05$).

170

171 **Predictions: MBA values and RC density**

172 To predict density values for groups of red colobus across the entire Mwanihana forest, we first
173 derived spatially diffused values for MBA from our best fitting averaged model, giving an MBA
174 value for each Landsat pixel in the entire study area. We removed those values of MBA that
175 appeared as outliers in the derived dataset (i.e. $>0.5m^2$). We believed these outliers were found for
176 those pixels where our model was not able to derive realistic MBA values, inside those areas close
177 to forest borders as well as in areas located at high elevation (above 1800 m), where trees are sparse
178 and are replaced by other vegetation (Lovett et al. 2006).

179

180 Besides MBA, previous modeling of red colobus group density was most effective using elevation
181 (negative sign) and distance from disturbance/forest edge (negative sign) (Cavada et al. 2016). We
182 therefore calculated spatially diffused values for these variables from a Digital Elevation Model
183 (DEM) and from a shapefile of the forest edge, respectively. We then used a published hierarchical

184 model (Cavada et al. 2016) to predict primate density across the Mwanihana forest using these two
185 variables and spatially diffused values for MBA derived from our model.
186 Finally, we verified the accuracy of our approach by comparing the predicted primate density to
187 density estimates in Cavada et al. (2016) for those plots in Barelli et al. (2015) (N=65) that were
188 excluded while building the MBA model (see 'Model building' above). These density estimates
189 were plot-specific values derived from the hierarchical analysis described above, and hence were
190 effectively the only field based and site-specific density estimates that could be used for such
191 validation. We compared observed and predicted values using OP regression (Piñeiro et al. 2008)
192 and we compared the slope and the intercept of the fitted model with the 1:1 line.

193

194 **Results**

195 After selecting the plots suitable for the analysis, we retained 61 plots from Barelli et al. (2015) and
196 54 TEAM sub-plots. Adding these to the 33 newly sampled plots, we obtained an overall dataset of
197 148 plots and their corresponding sampled MBA values. We built models using all the possible
198 combinations of the metrics and indices calculated from the Landsat images, including a null model.
199 We retained six competing models of MBA (Table 2) that were averaged for predictions. The
200 resulting average model retained the first and the second components of the PCA and the indices
201 RGI, RR and SLAVI (Table 3). This model showed adequate fit based on the bootstrap P value
202 based on the Chi-square statistic ($P=0.66$) and no significant difference between observed and
203 predicted MBA values ($W=602$, $P=0.92$). The MBA model failed to derive plausible values in those
204 areas located at high altitudes as well as close to the forest edge (Fig. 3). We obtained a spatially-
205 explicit map of estimated density of red colobus groups across the whole study area, as influenced
206 by the covariates MBA (predicted from our model and with a positive effect), elevation and distance
207 from disturbance (i.e from the forest edge), both with a negative effect, according to the hierarchical
208 model defined in Cavada et al. (2016) (Fig. 4).

209 The OP regression yielded a R^2 of 0.84 attesting the accuracy of the predicted red colobus group
210 density values as derived by using the spatially diffused values for MBA obtained from the GLM
211 analysis (Fig. 5).

212

213 **Discussion**

214 We have successfully predicted and mapped the spatial density of an endangered primate, hence
215 showing how modeling ecologically-relevant predictors of abundance can improve predictions on
216 species distribution (Franklin 1995), across a broad spatial extent. The species' density pattern
217 highlighted in our map is consistent with results in previous studies that were based solely on
218 ground data and hence with limited spatial inference (Struhsaker and Rovero 2007, Barelli et al.
219 2015, Cavada et al. 2016).

220

221 Our best supported models showed high accuracy in predicting MBA values, making it a reliable
222 tool for inference beyond the ground measurement sites, with a good level of confidence and
223 precision. MBA is a highly relevant descriptor of the canopy structure as well as a significant
224 covariate that has emerged in different studies as influential for predominantly arboreal primates
225 (Struhsaker and Rovero 2007, Cavada et al. 2016). As a parameter quantifying forest cover, MBA is
226 also a recognized proxy for habitat degradation and fragmentation (Urquiza-Haas et al. 2007). The
227 best fit model we derived from GLM retained the first two components of the PCA. This fitted the
228 acknowledged evidence that Landsat products are able to discriminate forested habitats, through the
229 information provided by specific spectral channels (Blair and Baumgardner 1977, Jakubauskas
230 1996, Eklundh et al. 2001, Cohen and Goward 2004), in terms of the differential reflectance emitted
231 by the higher strata of the canopy. The information provided by the Landsat sensors can highlight
232 specific vegetation components (Thenkabail et al. 2000, Almeida and De Souza Filo 2004); in fact
233 the bands of the visible spectrum and of the Short-wave Infrared (SWIR) can be correlated with
234 several forest structures, including basal area (Muukkonen and Heiskanen 2005, 2007, Hall et al.
235 2006). The relationship with MBA shown by the first PCA component of our model might be due to

236 a large presence of trees with great basal area and tall canopy, causing pronounced shadowing
237 which translates in a lower reflectance.

238

239 Among the vegetation indices retained by the models, RGI can be interpreted as a proxy of the
240 forest phenology by the time when the Landsat image was acquired. Since such an index provides
241 information on the ratio of red to green reflectance, the positive effect we found on MBA could be
242 due to the contribution the index generally gives in evaluating the size of the tree crowns, which is
243 related to the basal area extent. During that period, a high amount of trees shows indeed a
244 breakdown of green pigments and leaves fade from green to yellow and red (Motohka et al. 2010).
245 The positive effect we found for RR was also confirmed by other studies that found a correlation
246 between the visible and the SWIR band of the Landsat with several physical structures of the forest
247 canopy, including basal area (Muukkonen and Heiskanen 2005, Hall et al. 2006, Tonolli et al.
248 2011). In addition, the positive relationship we found between MBA and SLAVI index is not
249 surprising given that the index accounts for the sensitivity of the mid-infrared wavelength to the
250 structure of the canopy, especially for heterogeneous forest compositions (Lymburner et al. 2000).

251

252 As the main goal of our study, we used the predicted and spatially diffused values of MBA to derive
253 a map of the Udzungwa red colobus density. This matched, at a wider and spatially-diffuse scale,
254 the density estimates found in prior studies (Barelli et al. 2015; Cavada et al. 2016). In particular, it
255 confirmed the red colobus's preference for lower-elevation forest that are close to its edge, variably
256 disturbed and covered with regenerating vegetation, that is recognized as an important food source
257 for the species (Barelli et al. 2015). Densities decreased where MBA values increased, i.e. in the
258 interior and old growth forest parts and at higher elevation. This in turn indicates resilience of the
259 animal to anthropogenic disturbance and again the preference shown by the species for forest edges.
260 Such a counter intuitive density trend, is clearly visualized in the spatially explicit map we obtained.
261 This provides novel indications for the protection of forest areas that are located at the interface
262 with intense anthropogenic activity.

263

264 We have confirmed that the use of remote sensing represents a robust tool to improve model
265 performance and to reduce the costs of data collection (He et al. 2015), which implies bypassing the
266 sample size limits associated with field measurements. We stress the importance of carefully
267 evaluating the process regarding the selection of adequate satellite images, given the sensitivity for
268 seasonality shown by some vegetation indices. High resolution images should certainly be preferred
269 when deriving remote-sensing based predictor variables that can be essential to improve predictive
270 species modeling. Nonetheless, the quality of such images can often be poor, due to cloud coverage
271 that hides the underlying canopy, i.e. the carried amount of information is lower than the spectral
272 noise (Woodcock and Strahler 1987, Ricotta et al. 1999). This phenomenon consistently arises in
273 images of tropical mountain forests, since clouds accumulate relatively more in dense forest cover
274 areas due to evapotranspiration (Nagendra and Rocchini 2008). Still, we demonstrated that since
275 high resolution products in some cases cannot be used, medium resolution images like Landsat
276 proved to be an excellent source of data for applications both in the study of tropical forest structure
277 and to develop reliable species distribution models. However, caution is recommended regarding
278 the generalization of our approach, which is mainly relevant to comparable study systems in terms
279 of both habitat and target species characteristics.

280

281 **Conclusions**

282 Spatially explicit, predictive models of animal abundance can offer a powerful insight on the
283 species status and distribution, helping to identify those sites where urgent intervention is needed in
284 terms of protection and conservation. Overcoming the lack of high resolution and high quality
285 remote sensing products as well as of spatially diffused covariates of abundance is essential, as it
286 can firmly boost the usefulness of species distribution models. By focusing on the endangered
287 Udzungwa red colobus, we showed the potential of this approach to derive accurate spatially
288 diffused estimates of animal density and distribution. This approach is particularly suitable for
289 species for which data availability is incomplete and spatial coverage is heterogeneous, affecting the

290 capacity of developing site-specific conservation and restoration programs where urgent forest and
291 species protection is needed.

292

293 **Acknowledgements**

294 We thank the Tanzania Wildlife Research Institute (TAWIRI), Tanzania Commission for Science
295 and Technology (COSTECH), Tanzania National Parks (TANAPA) and the Tanzania Forest Service
296 (TFS) for granting us permissions to collect the new data for the study (Costech Permit No. 2015–
297 44– NA– 2015- 37 to N.C.). The new data collection for this study was funded by Rufford Small
298 Grants Foundation (1106-C to F.R.), and by MUSE-Museo delle Scienze and the University of
299 Trento to N.C. We thank L. Perathoner for providing helpful support and valuable suggestion for the
300 analysis of the Landsat dataset and for the implementation of the GRASS code. R. Laizzer and A.
301 Mwakisoma provided invaluable field assistance. We thank the Tropical Ecology Assessment and
302 Monitoring (TEAM) Network, a collaboration between Conservation International, the Smithsonian
303 Institute and the Wildlife Conservation Society, for providing part of the tree plot dataset; some of
304 these plots were in turn established through the Valuing the Arc programme and in collaboration
305 with J. Lovett, S. Lewis and P. Munishi. We thank H. Little for proof-reading the final version of the
306 manuscript and two anonymous reviewers for their relevant suggestions through the revision
307 process.

308

309

310

311

312

313

314

315

316

317 **References**

- 318 Alexander, R. R. 1971. Crown Competition Factor (CCF) for Engelmann Spruce in the Central
319 Rocky Mountains. Ed 1971 Forest Service, U.S. Dept. of Agriculture, Rocky Mountain Forest and
320 Range Experiment Station.
- 321 Almeida, T. I. R., and C. De Souza Filo. 2004. Principal component analysis applied to feature-
322 oriented band ratios of hyperspectral data: A tool for vegetation studies. *International Journal*
323 *of Remote Sensing* 25:5005–5023.
- 324 Anadón, J. D., A. Giménez, and R. Ballestar. 2010. Linking local ecological knowledge and habitat
325 modelling to predict absolute species abundance on large scales. *Biodiversity and*
326 *Conservation* 19:1443–1454.
- 327 Anderson, D. R., and K. P. Burnham. 2002. Avoiding pitfalls when using information-theoretic
328 methods. *The Journal of Wildlife Management* 66:912–918.
- 329 Anderson, J., G. Cowlshaw, and J. M. Rowcliffe. 2007. Effects of forest fragmentation on the
330 abundance of *Colobus angolensis palliatus* in Kenya's coastal forests. *International Journal of*
331 *Primates* 28:637–655.
- 332 Araldi, A., C. Barelli, K. Hodges, and F. Rovero. 2014. Density estimation of the endangered
333 Udzungwa red colobus (*Procolobus gordonorum*) and other arboreal primates in the Udzungwa
334 Mountains using systematic Distance Sampling. *International Journal of Primatology* 35:941–
335 956.
- 336 Arroyo-Rodríguez, V., and L. Fahrig. 2014. Why is a landscape perspective important in studies of
337 primates? *American Journal of Primatology* 909:901–909.
- 338 Balmford, A., and T. Whitten. 2003. Who should pay for tropical conservation, and how could the
339 costs be met? *Oryx* 37:238–250.
- 340 Barelli, C., R. Mundry, A. Araldi, K. Hodges, D. Rocchini, and F. Rovero. 2015. Modelling primate
341 abundance in complex landscapes: a case study from the Udzungwa Mountains of Tanzania.
342 *International Journal of Primatology* 36:209–226.
- 343 Barton, K. 2014. Multi-model inference. R package MuMIn version 1.10.5, 46.
- 344 Blair, B. O., and M. F. Baumgardner. 1977. Detection of the green and brown wave in hardwood
345 canopy covers using multivariate, multispectral data from LANDSAT-1. *Agronomy Journal* 69:
346 808–811.
- 347 Braithwaite, L. W., M. P. Austin, M. Clayton, J. Turner, and A. O. Nicholls. 1989. On predicting the
348 presence of birds in Eucalyptus forest types. *Biological Conservation* 50:33–50.
- 349 Brown, L., J. M. Chen, S. G. Leblanc, and J. Cihlar. 2000. A shortwave infrared modification to the
350 Simple Ratio for LAI retrieval in boreal forests: an image and model analysis. *Remote Sensing*
351 *of Environment* 71:16–25.
- 352 Cade, B. S. 1997. Comparison of tree basal area and canopy cover in habitat models: subalpine
353 forest. *Journal of Wildlife Management* 61:326–335.

- 354 Cavada, N., C. Barelli, M. Ciolli, and F. Rovero. 2016. Primates in human-modified and fragmented
355 landscapes: the conservation relevance of modelling habitat and disturbance factors in density
356 estimation. *Plos One* 11:e0148289.
- 357 Cayuela, L., D. Golicher, A. Newton, H. Kolb, F. S. de Albuquerque, E. J. M. M. Arets, J. R. M.
358 Alkemade, and A. M. Pérez. 2009. Species distribution modelling in the tropics: problems,
359 potentialities, and the role of biological data for effective species conservation. *Tropical*
360 *Conservation Science* 2:319–352.
- 361 Chen, J. M. 1996. Evaluation of vegetation indices and a modified Simple Ratio for boreal
362 applications. *Canadian Journal of Remote Sensing* 22:1–21.
- 363 Cohen, W. B. and S. N. Goward. 2004. Landsat's role in ecological applications of Remote Sensing.
364 *BioScience* 54:535–545.
- 365 Cohen, W. B., T. A. Spies, and M. Fiorella 1995. Estimating the age and structure of forests in a
366 multi-ownership landscape of western Oregon, U.S.A. *International Journal of Remote Sensing*
367 16:721–746.
- 368 Coops, N. C., M. Johnson, M. A. Wulder, and J. C. White 2006. Assessment of QuickBird high
369 spatial resolution imagery to detect red attack damage due to mountain pine beetle infestation.
370 *Remote Sensing of Environment* 103:67–80.
- 371 Cristóbal-Azkarate, J., J. J. Veà, N. Asensio, and E. Rodríguez-Luna. 2005. Biogeographical and
372 floristic predictors of the presence and abundance of mantled howlers (*Alouatta palliata*
373 *mexicana*) in rainforest fragments at Los Tuxtlas, Mexico. *American Journal of Primatology*
374 67:209–222.
- 375 Duncanson, L. I., K. O. Niemann, and M. A. Wulder. 2010. Integration of GLAS and Landsat TM
376 data for aboveground biomass estimation. *Canadian Journal of Remote Sensing* 36:129–141.
- 377 Eklundh, L., L. Harrie, and A. Kuusk. 2001. Investigating relationships between Landsat ETM+
378 sensor data and leaf area index in a boreal conifer forest. *Remote Sensing of Environment*
379 78:239–251.
- 380 Farr, W. A., D. J. DeMars, and J. E. Dealy. 1989. Height and crown width related to diameter for
381 open-grown western hemlock and Sitka spruce. *Canadian Journal of Forest Research* 19:
382 1203–1207.
- 383 Franklin, J. 1995. Predictive vegetation mapping: geographic modelling of biospatial patterns in
384 relation to environmental gradients. *Progress in Physical Geography* 19:474–499.
- 385 Gamon, J. A., and J. S. Surfus. 1999. Assessing leaf pigment content and activity with a
386 reflectometer. *New Phytologist* 143:105–117.
- 387 Gitelson, A. A., Y. J. Kaufman, and M. N. Merzlyak. 1996. Use of a green channel in remote
388 sensing of global vegetation from EOS-MODIS. *Remote Sensing of Environment* 58:289–298.
- 389 Guisan, A. and W. Thuiller. 2005. Predicting species distribution: offering more than simple habitat
390 models. *Ecology Letters* 8:993–1009.
- 391 Guisan, A., and N. E. Zimmermann. 2000. Predictive habitat distribution models in ecology.
392 *Ecological Modelling* 135:147–186.

- 393 Hair, J. F., B. Black, B. Babin, B., R. E. Anderson, and R. L. Tatham. 2006. *Multivariate Data*
394 *Analysis* 6th ed. Prentice Hall.
- 395 Hall, F. G., Y. E. Shimabukuro, and K. Huemmrich. 1995. Remote sensing of forest biophysical
396 structure using mixture decomposition and geometric reflectance models. *Ecological*
397 *Applications* 5:993–1013.
- 398 Hall, R. J., R. S. Skakun, E. J. Arsenault, and B. S. Case. 2006. Modelling forest stand structure
399 attributes using Landsat ETM+ data: application to mapping of aboveground biomass and
400 stand volume. *Forest Ecology and Management* 225:378–390.
- 401 Hardinsky, M. A., V. Klemas, and R. M. Smart. 1983. The influence of soil salinity, growth form
402 and leaf moisture on the spectral radiance of *Spartina alterniflora* canopies. *Photogrammetric*
403 *Engineering and Remote Sensing* 48:77-84.
- 404 He, K. S., B. A. Bradley, A. F. Cord, D. Rocchini, M. N. Tuanmu, S. Schmidlein, W. Turner, M.
405 Wegmann, and N. Pettorelli. 2015. Will remote sensing shape the next generation of species
406 distribution models? *Remote Sensing in Ecology and Conservation* 1:4-18.
- 407 Hédl, R., M. Svátek, M. Dančák, A. W. Rodzay, A. B. Salleh, and A. S. Kamariah. 2009. A new
408 technique for inventory of permanent plots in tropical forests: a case study from lowland
409 dipterocarp forest in Kuala Belalong, Brunei darussalam. *Blumea: Journal of Plant Taxonomy*
410 *and Plant Geography* 54:124–130.
- 411 IUCN. 2015. The IUCN Red List of Threatened Species. Version 2015-4. <www.iucnredlist.org>.
412 Downloaded on 08 March 2016.
- 413 Jackson, R. D., and A. R. Huete. 1991. Interpreting vegetation indices. *Preventive Veterinary*
414 *Medicine* 11:185–200.
- 415 Jakubauskas, M. E. 1996. Thematic mapper characterization of lodgepole pine seral stages in
416 Yellowstone National Park, USA. *Remote Sensing of Environment* 56:118–132.
- 417 Jordan, C. F. 1969. Derivation of leaf-area index from quality of light on the forest floor. *Ecology*
418 50:663–666.
- 419 Kennedy, P. 2008. *A Guide to Econometrics* 6th ed. Wiley-Blackwell.
- 420 Legaard, K. R., S. A. Sader, and E. M. Simons-Legaard. 2015. Evaluating the impact of abrupt
421 changes in forest policy and management practices on landscape dynamics: analysis of a
422 Landsat image time series in the Atlantic Northern Forest. *Plos One* 10:e0130428.
- 423 Lovett, J. C., A. R. Marshall, and J. Carr. 2006. Changes in tropical forest vegetation along an
424 altitudinal gradient in the Udzungwa Mountains National Park, Tanzania. *African Journal of*
425 *Ecology* 44:478-490.
- 426 Lymburner, L., P. Beggs, and C. Jacobson. 2000. Estimation of canopy-average surface-specific leaf
427 area using Landsat TM data. *Photogrammetric Engineering & Remote Sensing* 66:183–191.
- 428 Marquardt, D. W. 1970. Generalized inverses, Ridge regression, biased linear estimation, and
429 nonlinear estimation. *Technometrics* 12:591–612.

- 430 Marshall, A. R., H. I. O. Jørgensbye, F. Rovero, P. J. Platts, P. C. L. White, and J. C. Lovett. 2010.
431 The species-area relationship and confounding variables in a threatened monkey community.
432 *American Journal of Primatology* 72:325–336.
- 433 Marshall, A. R., S. Willcock, P. J. Platts, J. C. Lovett, A. Balmford, N. D. Burgess, J. E. Latham, P.
434 K. T. Munishi, R. Salter, D. D. Shirima, and S. L. Lewis. 2012. Measuring and modelling
435 above-ground carbon and tree allometry along a tropical elevation gradient. *Biological*
436 *Conservation* 154:20–33.
- 437 Mayes, M. T., J. F. Mustard, and J. M. Melillo. 2015. Forest cover change in Miombo Woodlands:
438 modelling land cover of African dry tropical forests with linear spectral mixture analysis.
439 *Remote Sensing of Environment* 165:203–215.
- 440 Mazerolle, M. J. 2015. R package “AICcmodavg” Model selection and multimodel inference
441 based on (Q)AIC(c).
- 442 Mbora, D. N. M., and D. B. Meikle. 2004. Forest fragmentation and the distribution, abundance and
443 conservation of the Tana river red colobus (*Procolobus rufomitratus*). *Biological Conservation*
444 118:67–77.
- 445 Medley, K. E. 1993. Primate conservation along the Tana River, Kenya: an examination of the
446 forest habitat. *Conservation biology* 7:109–121.
- 447 Motohka, T., K. N. Nasahara, H. Oguma, and S. Tsuchida. 2010. Applicability of Green-Red
448 Vegetation index for Remote Sensing of vegetation phenology. *Remote Sensing* 2:2369–2387.
- 449 Muukkonen, P., and J. Heiskanen. 2005. Estimating biomass for boreal forests using ASTER
450 satellite data combined with standwise forest inventory data. *Remote Sensing of Environment*
451 99:434–447.
- 452 Muukkonen, P., and J. Heiskanen. 2007. Biomass estimation over a large area based on standwise
453 forest inventory data and ASTER and MODIS satellite data: A possibility to verify carbon
454 inventories. *Remote Sensing of Environment* 107:617–624.
- 455 Nagendra, H., and D. Rocchini. 2008. High resolution satellite imagery for tropical biodiversity
456 studies: The devil is in the detail. *Biodiversity and Conservation* 17:3431–3442.
- 457 Nemani, R., L. Pierce, S. Running, and L. Band. 1993. Forest ecosystem processes at the watershed
458 scale: sensitivity to remotely-sensed Leaf Area Index estimates. *International Journal of*
459 *Remote Sensing* 14:2519–2534.
- 460 Ota, T., O. Ahmed, S. Franklin, M. Wulder, T. Kajisa, N. Mizoue, S. Yoshida, G. Takao, Y. Hirata,
461 N. Furuya, T. Sano, S. Heng, and M. Vuthy. 2014. Estimation of airborne Lidar-derived
462 tropical forest canopy height using Landsat time series in Cambodia. *Remote Sensing*
463 6:10750–10772.
- 464 Piñeiro, G., S. Perelman, J. P. Guerschman, and J. M. Paruelo. 2008. How to evaluate models:
465 observed vs. predicted or predicted vs. observed? *Ecological Modelling* 216:316–322.
- 466 Platts, P. J., N. D. Burgess, R. E. Gereau, J. C. Lovett, A. R. Marshall, C. J. Mc Clean, P. K. E.
467 Pellikka, R. D. Swetnam, and R. Marchant. 2011. Delimiting tropical mountain ecoregions for
468 conservation. *Environmental Conservation* 38:312–324.

- 469 Proisy, C., P. Coutron, and F. Fromard. 2007. Predicting and mapping mangrove biomass from
470 canopy grain analysis using Fourier-based textural ordination of IKONOS images. *Remote*
471 *Sensing of Environment* 109:379–392.
- 472 R Core Team. 2015. R: A language and environment for statistical computing. R Foundation for
473 Statistical Computing, Vienna, Austria. URL <https://www.R-project.org/>.
- 474 Ricotta, C., G. C. Avena, and F. Volpe. 1999. The influence of principal component analysis on the
475 spatial structure of a multispectral dataset. *International Journal of Remote Sensing* 20:3367–
476 3376.
- 477 Rouse, J. W., R. H. Haas, J. A. Schell, W. D. Deering, and J. C. Harlan. 1974. Monitoring the vernal
478 advancement and retrogradation (greenwave effect) of natural vegetation. Technical report,
479 NASA, United States.
- 480 Schipper, J., et al. 2008. The status of the world's land and marine mammals: diversity, threat, and
481 knowledge. *Science* 322:225–230.
- 482 Schroeder, T. A., M. A. Wulder, S. P. Healey, and G. G. Moisen. 2011. Mapping wildfire and
483 clearcut harvest disturbances in boreal forests with Landsat time series data. *Remote Sensing*
484 *of Environment* 115:1421–1433.
- 485 Schwitzer, C., R. A. Mittermeier, A. B. Rylands, F. Chiozza, E. A. Williamson, J. Wallis, and
486 Cotton, A., editors. 2015. *Primates in Peril: The World's 25 Most Endangered Primates 2014-*
487 *2016*. IUCN SSC Primate Specialist Group (PSG), International Primatological Society (IPS),
488 Conservation International (CI), and Bristol Zoological Society, Arlington, VA. iv+93pp.
- 489 Smith, W. R., R. M. Farrar Jr., P. A. Murphy, J. L. Yeiser, R. S. Meldahl, and J. S. Kush. 1992.
490 Crown and basal area relationships of open-grown southern pines for modelling competition
491 and growth. *Canadian Journal of Forest Research* 22:341–347.
- 492 Steel, R. I. 2012. The effects of habitat parameters on the behavior, ecology, and conservation of the
493 Udzungwa red colobus monkey (*Procolobus gordonorum*). Graduate School of Duke
494 University PhD thesis, Department of Biological Anthropology and Anatomy, Duke
495 University.
- 496 Struhsaker, T. T., and F. Rovero. 2007. Vegetative predictors of primate abundance: utility and
497 limitations of a fine-scale analysis. *American Journal of Primatology* 69:1242–1256.
- 498 TEAM Network. 2011. Terrestrial vertebrate protocol implementation manual, v. 3.1. Tropical
499 Ecology, Assessment and Monitoring Network, Center for applied biodiversity science,
500 Conservation International, Arlington, VA, USA.
- 501 Thenkabail, P. S., R. B. Smith, and E. De Pauw. 2000. Hyperspectral vegetation indices and their
502 relationships with agricultural crop characteristics. *Remote Sensing of Environment* 71:158–
503 182.
- 504 Tonolli, S., M. Dalponte, M. Neteler, M. Rodeghiero, L. Vescovo, and D. Gianelle. 2011. Fusion of
505 airborne LiDAR and satellite multispectral data for the estimation of timber volume in the
506 Southern Alps. *Remote Sensing of Environment* 115:2486–2498.

- 507 Twongyirwe, R., M. Bithell, K. S. Richards, and W. G. Rees. 2015. Land use policy three decades of
508 forest cover change in Uganda's Northern Albertine Rift Landscape. *Land Use Policy* 49:
509 236–251.
- 510 Umopathy, G., and A. Kumar. 2000. The occurrence of arboreal mammals in the rain forest
511 fragments in the Anamalai Hills, South India. *Biological Conservation* 92:311–319.
- 512 Urquiza-Haas, T., P. M. Dolman, and C. A. Peres. 2007. Regional scale variation in forest structure
513 and biomass in the Yucatan Peninsula, Mexico: effects of forest disturbance. *Forest Ecology
514 and Management* 247:80–90.
- 515 Vescovo, L., and D. Gianelle. 2008. Using the MIR bands in vegetation indices for the estimation of
516 grassland biophysical parameters from satellite remote sensing in the Alps region of Trentino
517 (Italy). *Advances in Space Research* 41:1764–1772.
- 518 Wilkie, D. S., and J. T. Finn. 1996. *Remote sensing imagery for natural resources monitoring: a
519 guide for first-time users.* Columbia University Press.
- 520 Woodcock, C. E., and A. H. Strahler. 1987. The factor of scale in remote sensing. *Remote Sensing
521 of Environment* 21:311–332.
- 522 Wulder, M. A., and S. E. Franklin. 2006. *Understanding forest disturbance and spatial pattern,
523 Remote Sensing and GIS approaches.* CRC Press.
- 524
525
526
527
528
529
530
531
532
533
534
535
536
537
538
539
540
541
542
543
544
545
546
547
548

549 **Tables**

550

551 **Table 1.** Vegetation indices extracted from a Landsat 8 image for comparison to ground sampled
 552 measures of mean basal area (MBA).

Index	Algorithm	Description	References
Simple Ratio (SR)	$SR = \rho_{nir}/\rho_{red}$	Index related to changes in the amount of green vegetation; reduces the effect of atmosphere and topography.	(Jordan 1969)
Corrected Simple Ratio (SRC)	$SRC = SR (1 - ((\rho_{mir} - \rho_{mir\ min}) / (\rho_{mir\ max} - \rho_{mir\ min})))$	Linearizes the relationships with parameters, accounting for MIR band.	(Brown et al. 2000)
Normalized Difference Vegetation Index (NDVI)	$NDVI = (\rho_{nir} - \rho_{red}) / (\rho_{nir} + \rho_{red})$	Estimates the amount of vegetation, it assumes values that are normalized for the amount of incident radiation.	(Rouse et al. 1974)
Corrected Normalized Difference Vegetation Index (NDVIC)	$NDVIC = NDVI (1 - ((\rho_{mir} - \rho_{mir\ min}) / (\rho_{mir\ max} - \rho_{mir\ min})))$	Linearizes the relationships with parameters, accounting for MIR band	(Nemani et al. 1993)
Modified Simple Ratio (MSR)	$MSR = (\rho_{nir}/\rho_{red} - 1) / ((\rho_{nir}/\rho_{red})^{1/2} + 1)$	Linearizes the	(Chen 1996)

		relationship between the index and biophysical parameters	
Reflectance Ratio (RR)	$RR = \rho_{\text{mir}} / \rho_{\text{red}}$	Substitutes NIR band in SR with MIR band, which is more sensitive in distinguishing complex and stratified forest structures	(Tonolli et al. 2011)
Normalized Difference Water Index (NDWI)	$NDWI = (\rho_{\text{nir}} - \rho_{\text{mir}}) / (\rho_{\text{nir}} + \rho_{\text{mir}})$	Sensitive to vegetation water	(Hardinsky et al. 1983)
Specific Leaf Area Vegetation Index (SLAVI)	$SLAVI = \rho_{\text{nir}} / (\rho_{\text{red}} + \rho_{\text{mir}})$	Estimates Specific Leaf Area	(Lymburner et al. 2000)
Red Green Ratio (RGR)	$RGR = \rho_{\text{red}} / \rho_{\text{green}}$	Sensitive to different foliar pigments	(Gamon and Surfus 1999)
Red Green Index (RGI)	$RGI = (\rho_{\text{green}} - \rho_{\text{red}}) / (\rho_{\text{green}} + \rho_{\text{red}})$	Normalization of RGR results	(Coops et al. 2006)
Green Normalized Difference Vegetation Index (GNDVI)	$GNDVI = (\rho_{\text{nir}} - \rho_{\text{green}}) / (\rho_{\text{nir}} + \rho_{\text{green}})$	Estimates the amount of green vegetation, exploiting the green channel, sensitive to chlorophyll	(Gitelson et al. 1996)
Normalized Canopy Index (NCI)	$NCI = (\rho_{\text{mir}} - \rho_{\text{green}}) / (\rho_{\text{mir}} + \rho_{\text{green}})$	Linearizes the relationships with parameters, accounting for MIR	(Vescovo and Gianelle 2008)

and green bands

Tasseled Cap Angle (TCA) $TCA = \arctan(TCG/TCB)$ Index based on the (Powell et al. 2010)

angle formed by

brightness (TCB) and

greenness (TCG) in

the vegetation plane,

calculated from TCT

(Tasseled Cap Trans-

formation)

553

554

555

556

557

558

559

560

561

562

563

564

565

566

567

568

569

570

571

572 **Table 2.** Akaike Information Criterion (AIC) value for high ranked models ($\Delta\text{AIC}<2$) of mean basal
 573 area (MBA) modeled as a function of predictors derived from a Landsat 8 image.

Model	AIC	ΔAIC
MBA~P1+RGI	-620.70	0
MBA~P1+RGI+RR	-619.89	0.81
MBA~P1+SLAVI	-619.46	1.24
MBA~P1	-619.097	1.607
MBA~P1+P2+RGI	-619.096	1.609
MBA~P1+RR+SLAVI	-618.98	1.72

574 P1=First component of the Principal Component Analysis; P2= Second component of the Principal
 575 Component Analysis; RGI=Red Green Index; RR=Red Ratio; SLAVI=Specific Leaf Area
 576 Vegetation Index.

577

578

579

580

581

582

583

584

585

586

587

588

589

590

591

592 **Table 3.** Estimates and standard errors for the parameters retained in the averaged model for mean
 593 basal area (MBA) modeled as a function of metrics and indices extracted from a Landsat 8 image.

Model-averaged coefficients	Estimate	SE	p
P1	-37.92	19.61	0.05
RGI	31.71	15.43	0.04
RR	19.40	16.45	0.2
SLAVI	27.09	16.18	0.09
P2	18.15	24.64	0.4

594 P1=First component of the Principal Component Analysis; P2= Second component of the Principal
 595 Component Analysis; RGI=Red Green Index; RR=Red Ratio; SLAVI=Specific Leaf Area
 596 Vegetation Index.

597

598

599

600

601

602

603

604

605

606

607

608

609

610

611

612

613 **Figures**

614

615

616

617

618

619

620

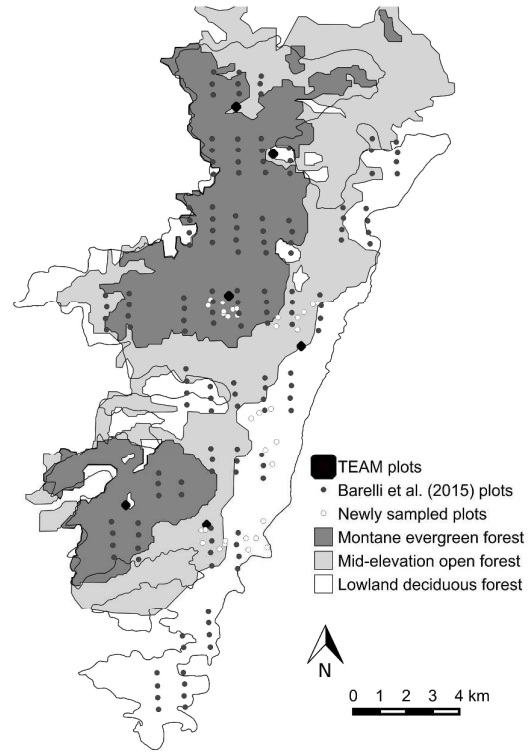
621

622

623

624

625



626 **Fig. 1.** Map of Mwanihana forest in the Udzungwa Mountains of Tanzania showing the distribution
627 of three vegetation plots data-sets used to derive basal area.

628

629

630

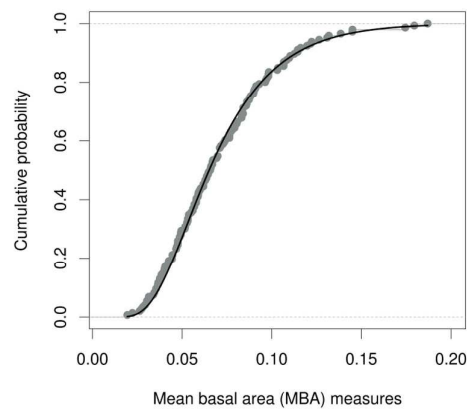
631

632

633

634

635



636 **Fig. 2.** Empirical cumulative distribution function of ground sampled measures of mean basal area
637 (MBA, gray dots) collected at tree plots in Mwanihana forest, Udzungwa Mountains, Tanzania. The
638 black line shows the fit of the theoretical inverse Gaussian distribution.

639

640

641

642

643

644

645

646

647

648

649

650

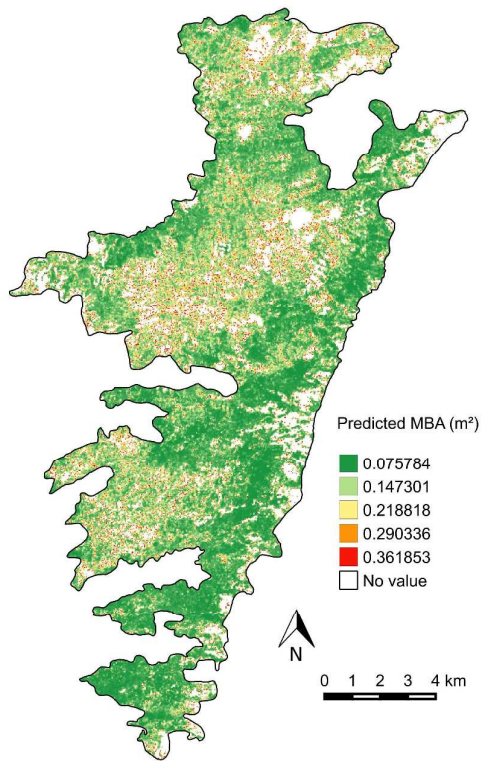
651

652

653

654

655
656
657
658
659
660
661
662
663
664
665
666



667 **Fig. 3.** Predicted values of mean basal area (MBA) across Mwanihana forest using the average
668 model of ground sampled values versus Landsat 8 metrics. White areas show pixels where the
669 model failed to predict plausible values of MBA (i.e. <math><0.5\text{m}^2</math>).

670

671

672

673

674

675

676

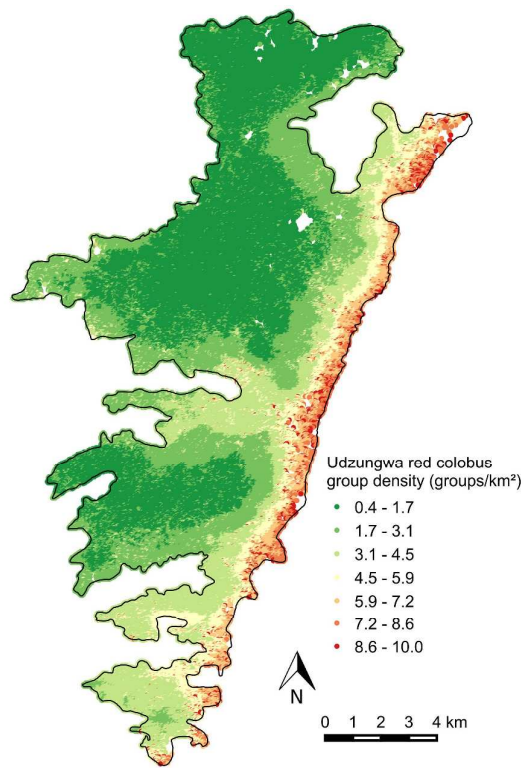
677

678

679

680

681



682 **Fig. 4.** Predicted Udzungwa red colobus group density in Mwanihana forest using a species density

683 model (Cavada et al. 2016) derived from remotely sensed mean basal area.

684

685

686

687

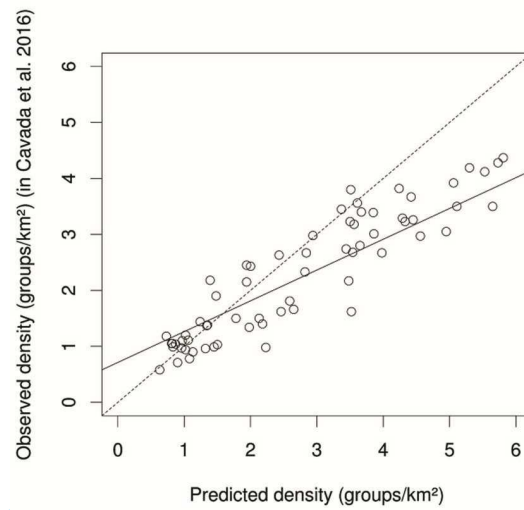
688

689

690

691

692



693 **Fig. 5.** Linear regression (dotted line) of observed versus predicted values of Udzungwa red colobus
694 density (groups/km²) among test vegetation plots (N=66). A 1:1 relationship is indicated by the
695 solid line.

696

697

698

699

700

701

702

703

704

705

706

707

708

709

710

711 **Supporting information**

712 **Data S1.** Summary of the dataset regarding the field sampled vegetation

713 **Data S2.** Code for the GRASS 7.0 module that was implemented to derive a series of vegetation

714 indices, combining specific bands of a Landsat 8 image.

For Review Only

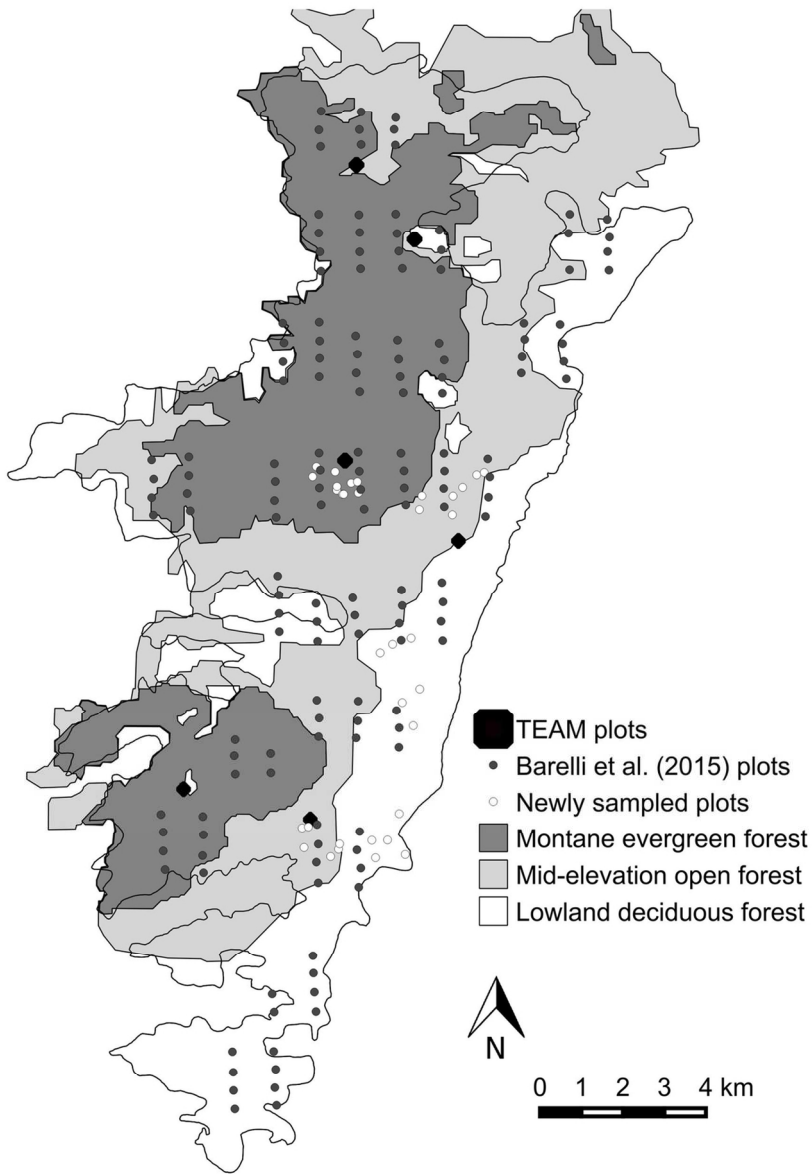


Fig. 1. Map of Mwanihana forest in the Udzungwa Mountains of Tanzania showing the distribution of three vegetation plots data-sets used to derive basal area.

107x152mm (300 x 300 DPI)

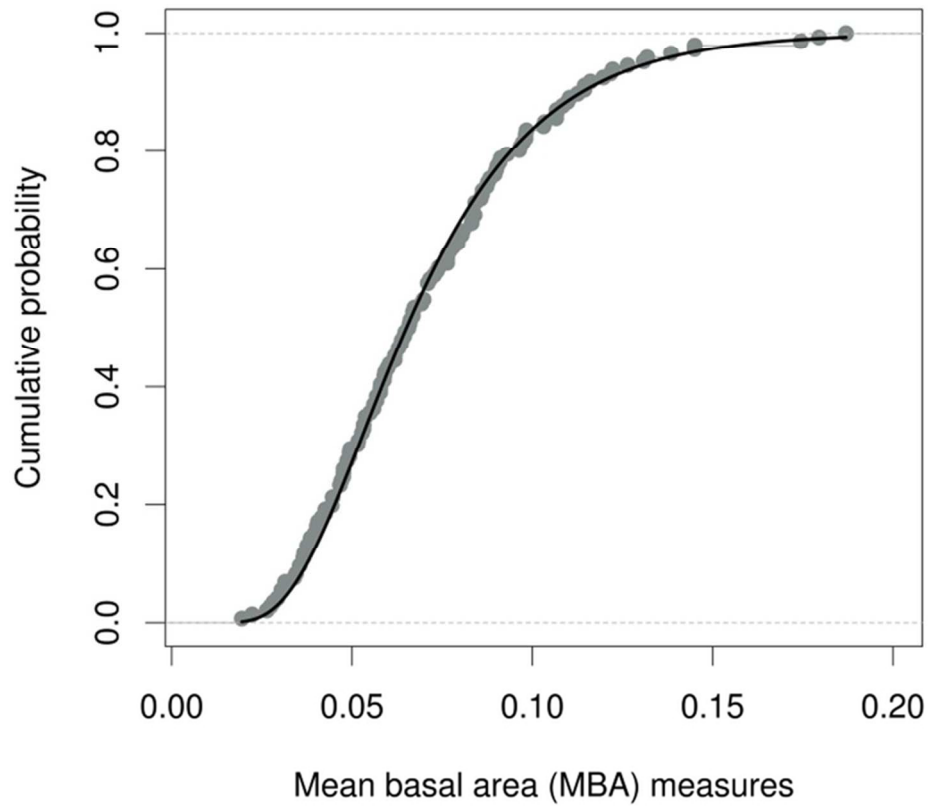


Fig. 2. Empirical cumulative distribution function of ground sampled measures of mean basal area (MBA, gray dots) collected at tree plots in Mwanihana forest, Udzungwa Mountains, Tanzania. The black line shows the fit of the theoretical inverse Gaussian distribution.

70x70mm (300 x 300 DPI)

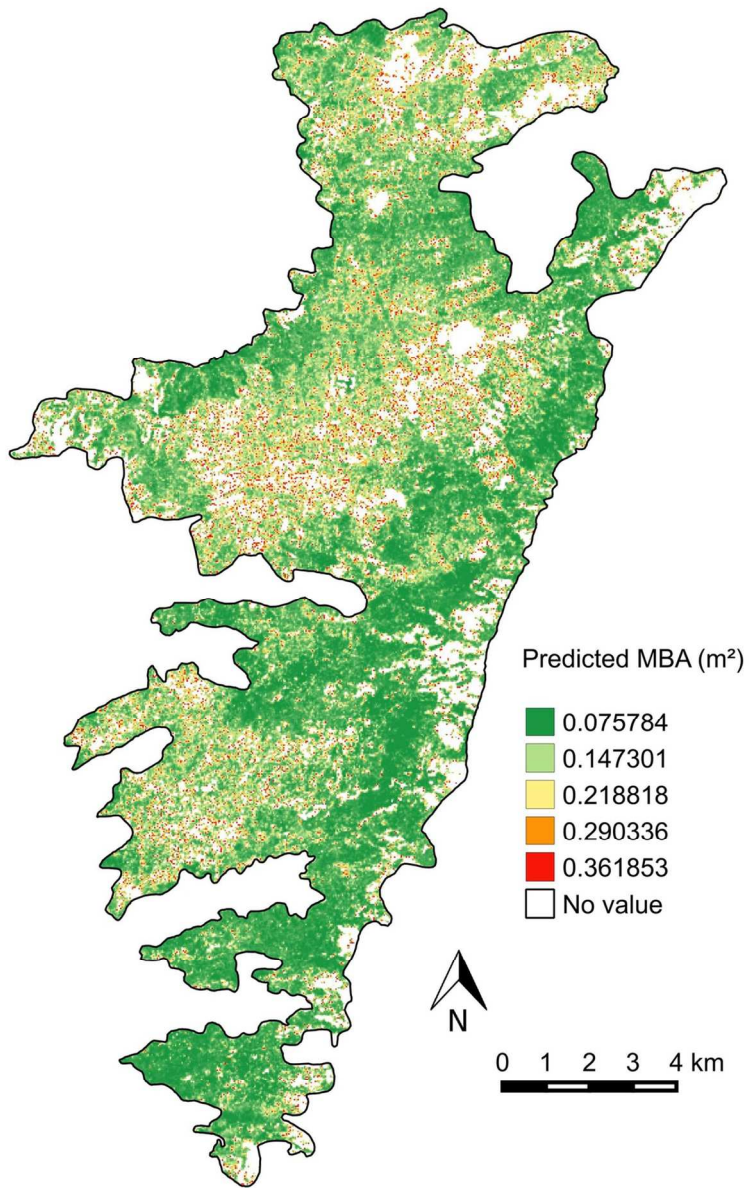


Fig. 3. Predicted values of mean basal area (MBA) across Mwanihana forest using the average model of ground sampled values versus Landsat 8 metrics. White areas show pixels where the model failed to predict plausible values of MBA (i.e. <math><0.5\text{m}^2</math>).

107x152mm (300 x 300 DPI)

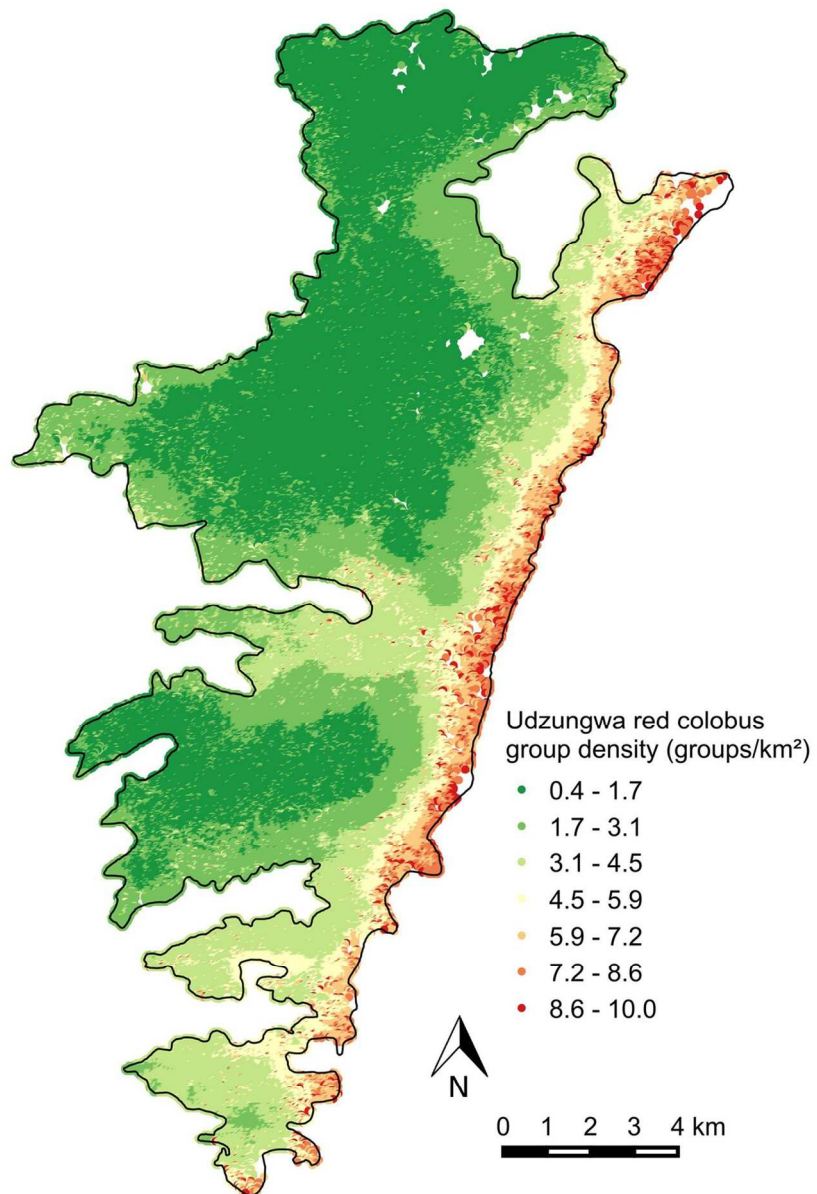


Fig. 4. Predicted Udzungwa red colobus group density in Mwanihana forest using a species density model (Cavada et al. 2016) derived from remotely sensed mean basal area.

107x152mm (300 x 300 DPI)

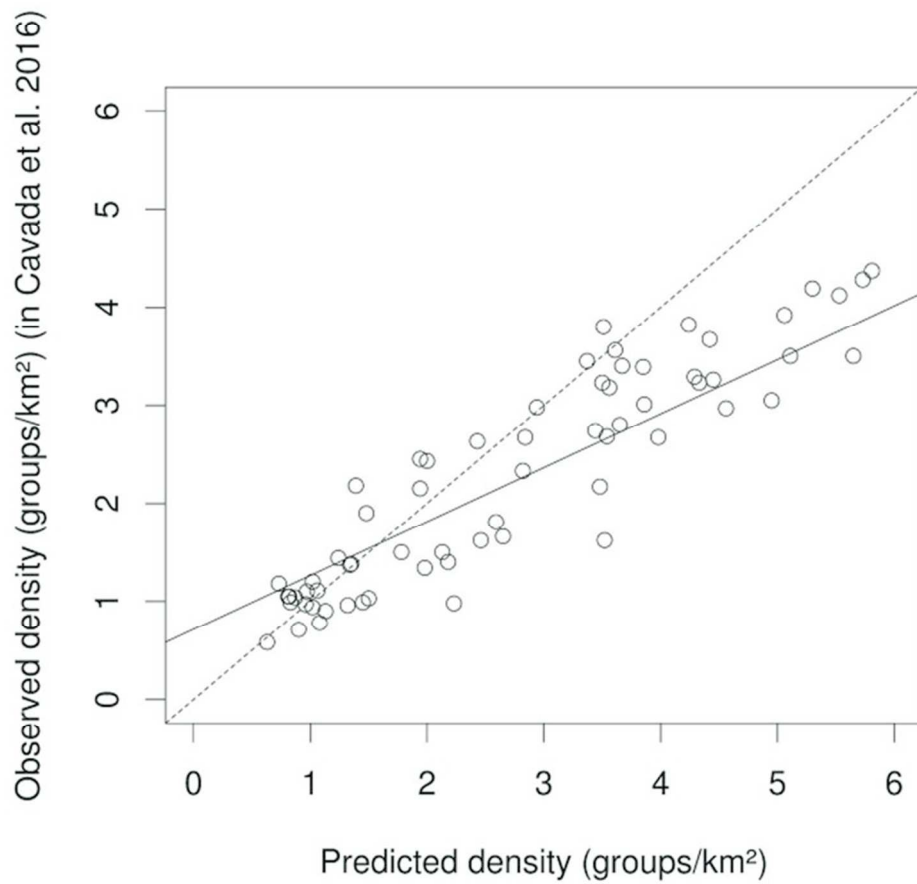


Fig. 5. Linear regression (dotted line) of observed versus predicted values of Udzungwa red colobus density (groups/km²) among test vegetation plots (N=66). A 1:1 relationship is indicated by the solid line.

76x76mm (300 x 300 DPI)

S1 Metadata

Data set: ID for the data set source

DBH: Diameter at breast height, measured for all the tree stems having diameter ≥ 10 cm

Basal area: $BA = \pi * (DBH/2)^2$

Climber: visually estimated coverage of climbers on trees as proportion of volume of the canopy, using 5 classes (0,25,50,75,100%).

Canopy: visually estimated extent of canopy cover, using 5 classes (0,25,50,75,100%)

For Review Only

```
#!/usr/bin/env python
#%module
#% description: Calculates vegetation indices for Landsat TM/ETM+/OLI spectral
bands
#% keywords: landsat, vegetation, indices, spectral, bands
#%end

#%option
#% key: band_prefix
#% type: string
#% gisprompt: old,cell,raster
#% description: Base name of input raster bands or a raster band map
#% required: yes
#%end

#%option
#% key: indices_prefix
#% type: string
#% description: Prefix for output raster indices maps
#% answer: spectral
#% required : yes
#%end

#%flag
#% key: t
#% description: Use bands for LANDSAT-4,5,7 (TM/ETM+)
#%END

#%flag
#% key: o
#% description: Use bands for LANDSAT-8 (OLI)
#%END

#%flag
#% key: c
#% description: Calculates also Cap Tassellation Indices
#%END

#%option
#% key: tc_prefix
#% type: string
#% gisprompt: old,cell,raster
#% description: If c flag: base name of input Tasselled Cap or a Tasselled Cap
map
#% required: no
#%end

#%Option
#% key: sensor
#% type: string
#% required: yes
#% multiple: no
#% options: LANDSAT-4;5;7 (TM/ETM+),LANDSAT-8 (OLI)
#% description: Use bands for sensor
#% answer: LANDSAT-8 (OLI)
#%End

import os, sys, shutil
import os.path, re
import grass.script as g

def main():

    #r.mapcalc float coercing with integer input
```

```

#(dn_B6-dn_B4)/(dn_B6+dn_B4)
#1.0*(dn_B6-dn_B4)/(dn_B6+dn_B4)
#(1.0*dn_B6-1.0*dn_B4)/(1.0*dn_B6+1.0*dn_B4)
#(float(dn_B6)-float(dn_B4))/(float(dn_B6)+float(dn_B4))

# define indices formulas

# RR: SWIR/Red reflectance ratio
rr_expr = '%(outpref)s_rr =1.0* %(mir)s / %(r)s'

# SR: Simple ratio NIR/Red reflectance ratio (Jordan, 1969)
sr_expr = '%(outpref)s_sr =1.0* %(nir)s / %(r)s'

# SRc: Corrected Simple Ratio (Brown et al. 2000)
src_expr = '%(outpref)s_src =1.0* $sr *(1-((%(mir)s -
%(minmir)s)/(%(maxmir)s - %(minmir)s)) )'

# MSR: Modified Simple Ratio (Chen, 1996)
msr_expr = '%(outpref)s_msr =1.0* ((%(nir)s / %(r)s -1)/(sqrt(%(nir)s /
%(r)s)+1))'

# RGR: Red Green Ratio (Gamon and Surfus)
rgr_expr = '%(outpref)s_rgr =1.0* %(r)s / %(g)s'

# RGI: Red Green Index (Coops et al.)
rgi_expr = '%(outpref)s_rgi =1.0* ((%(g)s - %(r)s)/(%(g)s + %(r)s))'

# NDVI: Normalized Difference Vegetation Index (Rouse et al., 1974)
ndvi_expr = '%(outpref)s_ndvi =1.0* ((%(nir)s - %(r)s)/(%(nir)s + %(r)s))'

# NDVIc: Corrected NDVI (Nemani et al., 1993)
ndvic_expr = '%(outpref)s_ndvic =1.0* $ndvi *(1-((%(mir)s -
%(minmir)s)/(%(maxmir)s - %(minmir)s)) )'

# GNDVIgreen: NGreen Normalized Difference Vegetation Index (Gitelson et
al., 1996)
gndvi_expr = '%(outpref)s_gndvi =1.0* ((%(nir)s - %(g)s)/(%(nir)s + %(g)s))'

# NDWI: Normalized Difference Water Index (Gao, 1996)
ndwi_expr = '%(outpref)s_ndwi =1.0* ((%(nir)s - %(mir)s)/(%(nir)s +
%(mir)s))'

# SLAVI: Specific Leaf Area Vegetation Index (Lymburner et al., 2000)
slavi_expr = '%(outpref)s_slavi =1.0* %(nir)s /((%(r)s + %(mir)s))'

# NCI: Normalized Canopy Index (Vescovo & Gianelle, 2008)
nci_expr = '%(outpref)s_nci =1.0* ((%(mir)s - %(g)s)/(%(mir)s + %(g)s))'

# NBR: Normalized Burn Ratio -> NOT IMPLEMENTED
# fire/burn index, use TM7/OLI_SWIR2

# TCA: Tasselled Cap Angle (Powell et al., 2010; Gomez et al., 2011)
tca_expr = '%(outpref)s_tca =1.0* atan(%(gr)s / %(br)s)' #deg angle

# ln(-We)
lnmwe_expr = '%(outpref)s_lnmwe =1.0* log(-%(we)s)'

# MAIN
landname= options['band_prefix'] #'toare_B'

```

```

indicespref= options['indices_prefix'] #'spectral'

#remove path before names and anything aftre the last point (ext)
#landpref=os.path.splitext(os.path.basename(landname))[0]

#remove ending numer from basename (purge path and @mapset)
#BASH: echo $(basename $landname) | sed 's/[0-9]*$//'
landpref=re.sub('[0-9]*$', '',os.path.basename(landname.split('@')[0]))

# define bands maps
if flags['o']:
    #landsat8
    g.message("OLI sensor")
    blue=landpref+'2'
    green=landpref+'3'
    red=landpref+'4'
    ninfrar=landpref+'5'
    minfrar=landpref+'7' #SWIR1
elif flags['t']:
    #landsat7
    g.message("TM/ETM+ sensor")
    blue=landpref+'1'
    green=landpref+'2'
    red=landpref+'3'
    ninfrar=landpref+'4'
    minfrar=landpref+'5'
else:
    #landsat8
    g.message("Warning: no sensor specified, defaout OLI used")
    blue=landpref+'2'
    green=landpref+'3'
    red=landpref+'4'
    ninfrar=landpref+'5'
    minfrar=landpref+'7' #SWIR1

#set region on a band map (are all equal)
g.run_command('g.region', rast = minfrar)

# mir max and min
min_mir = g.raster_info(minfrar)['min']
max_mir = g.raster_info(minfrar)['max']

bands= {
    "outpref" : indicespref,
    "b" : blue,
    "g" : green,
    "r" : red,
    "nir" : ninfrar,
    "mir" : minfrar,
    "minmir" : min_mir,
    "maxmir" : max_mir,
}

# compute indices with GRASS mapcalc
g.message("Calculating vegetation indices")
g.mapcalc(rr_expr % bands, overwrite = True)
g.mapcalc(sr_expr % bands, overwrite = True)
g.mapcalc(src_expr % bands, sr=indicespref+'_sr', overwrite = True)
g.mapcalc(msr_expr % bands, overwrite = True)
g.mapcalc(rgr_expr % bands, overwrite = True)

```

```

g.mapcalc(rgi_expr % bands, overwrite = True)
g.mapcalc(ndvi_expr % bands, overwrite = True)
g.mapcalc(ndvic_expr % bands, ndvi=indicespref+'_ndvi', overwrite = True)
g.mapcalc(gndvi_expr % bands, overwrite = True)
g.mapcalc(ndwi_expr % bands, overwrite = True)
g.mapcalc(slavi_expr % bands, overwrite = True)
g.mapcalc(nci_expr % bands, overwrite = True)

if flags['c']:
    tcname= options['tc_prefix']
    if tcname=="":
        g.message("Warning: no TC prefix, defaout 'tct8_C.' used")
        tcpref='tct8_C.'
    else:
        tcpref=re.sub('[0-9]*$',
'',os.path.basename(tcname.split('@')[0]))

    comp= {
        "outpref" : indicespref,
        "br" : tcpref+'1',
        "gr" : tcpref+'2',
        "we" : tcpref+'3',
    }

    g.message("Calculating Cap Tassellation indices")
    g.mapcalc(tca_expr % comp, overwrite = True)
    #g.mapcalc(lnmwe_expr % comp, overwrite = True) #null() 4 We>0

return 0
#End main

if __name__ == "__main__":
    options, flags = g.parser()
    sys.exit(main())

```